# Performance of Artificial Bed-Wetting Parameter in a 1D Coulomb-Type Debris Flow Numerical Model

**Van Khoi Pham**
Faculty of Civil Engineering, Vietnam Maritime University, Hai Phong City, Viet Nam
khoipv.ctt@vimaru.edu.vn (corresponding author)

*Received: 25 February 2025 | Revised: 12 March 2025 | Accepted: 18 March 2025*

 *DOI: https://doi.org/10.48084/etasr.10719*

## ABSTRACT

**Debris flow, which usually occurs after a landslide event, can damage human property along its trajectory, especially when the flow front moves at high speed. Coulomb resistance flow is considered the fastest type of flow due to the inclusion of the only internal friction component in the source term of the numerical model. Additionally, in the one-dimensional (1D) Coulomb-type numerical solution, an artificial bed-wetting parameter is required to ensure model stability in dry areas. This study aimed to evaluate the performance of artificial bed-wetting parameters in terms of debris velocity and debris depth with various slope and friction angles in the 1D Coulomb-type debris flow numerical model. The analytical solution of the Coulomb resistance flow is used to quantify the accuracy of the numerical results obtained with different artificial bed-wetting parameters. Five cases of debris dam-break tests are investigated to evaluate the influence of artificial bed-wetting parameters on slope and internal friction angles through debris variables. The results show that debris depth and debris front velocity are more accurate with smaller values of the artificial bed-wetting parameter, larger slope angles, and smaller internal friction angles. Furthermore, an inverse relationship between slope angle and debris front velocity, and a reverse relationship between internal friction angle and debris front velocity, are identified as fundamental physical flow properties.**

***Keywords-debris flow; Coulomb resistance; artificial bed-wetting; numerical model***

## I. INTRODUCTION

Due to gravitational force, rapid landslides or avalanches can trigger debris flows, which propagate along their paths and accumulate on flatbeds [1-6]. These debris flows, composed of materials such as rock, soil, wood, or snow, can cause significant damage to human infrastructure and pose a threat to human life [3, 5, 7]. Debris flows occur frequently in mountainous regions at very high speeds, making it difficult to collect real field data [1, 7]. Consequently, researchers focus on laboratory experiments [8, 9] and numerical simulations [2, 10-12]. Compared to physical experiments, numerical simulations save time and costs and offer greater flexibility and scalability.

The first numerical model of debris was introduced in [1], using the finite difference method to solve nonlinear shallow water equations that incorporate the Coulomb resistance in the source term. Later, in [13], an analytical solution was developed for Coulomb-type nonlinear shallow-water equations. Subsequently, in [14], this analytical solution of Coulomb friction was applied to test a high-resolution finite-volume method in a 1D debris flow model. Several researchers have since used this Coulomb-type analytical solution to validate their finite-volume numerical debris flow models [12, 15]. In numerical models of debris flow, the Coulomb-type friction law is often used for dry granular flows, such as rockfalls [1] and dense snow avalanches [13]. Depending on the solid-fluid mixture, the yield strength, Coulomb friction, or turbulent resistance are considered in the friction terms of the source term in the momentum equation [2].

The fundamental difference between the finite difference and finite-volume schemes lies in the treatment of physical variables. While the finite difference scheme directly uses variables such as depth (e.g., $h$ in meters) and particle velocity (e.g., $u$ in m/s), the finite volume scheme solves for particle velocity using depth and unit discharge (e.g., $hu$ in $m^2/s$). Usually, in debris flow phenomena, the region filled with debris is the wet region, while the empty region is the dry region. To avoid division by zero errors in dry regions of the debris domain, a small depth value is introduced, known as the artificial bed-wetting parameter ($\varepsilon$) [16]. Various researchers have employed this parameter in their finite-volume scheme, often specifying a value of $10^{-6}$ m or smaller [17-21]. However, many of these studies did not utilize only Coulomb-type friction as a source term in the governing equations. Even in the finite difference framework in [1], artificial viscosity was necessary to maintain numerical stability when calculating the particle velocity. To date, no study has systematically analyzed the accuracy of numerical results for different values of the artificial bed-wetting parameter.

This study examines the performance of artificial bed-wetting parameters in numerical results in comparison to the analytical solution in [13], utilizing the same Coulomb-type resistance in a 1D nonlinear shallow-water debris flow model. The results include debris depth and particle velocity for various values of bottom slope angles and internal friction angles across different artificial bed-wetting parameters. This research also finds relationships between slope angles, friction angles, and particle velocity.

## II. MODEL DESCRIPTION

This section introduces, the 1D debris flow numerical model including governing equations, Coulomb resistance, numerical method, and artificial bed-wetting parameter.

### A. Governing equations

Figure 1 shows variables of debris flow on non-erodible beds after triggering landslides.

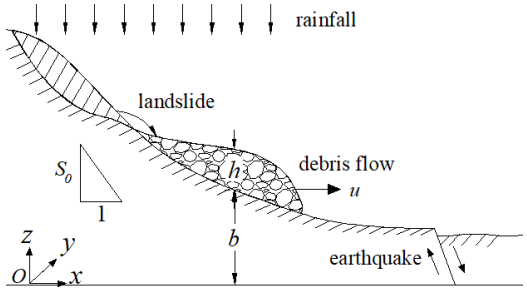


Fig. 1. Schematic of debris flow in terms of landslide generation.

By integrating the Navier-Stokes equations in depth, the continuity and momentum equations of the nonlinear shallow water equations [12, 14] are expressed as follows:

$$\frac{\partial h}{\partial t} + \frac{\partial (hu)}{\partial x} = 0 \quad (1)$$

$$\frac{\partial (hu)}{\partial t} + \frac{\partial (hu^2)}{\partial x} + \frac{1}{2} g \frac{\partial h^2}{\partial x} = gh(S_0 - S_f) \quad (2)$$

where $h$ is the debris flow depth, $u$ is the particle debris flow velocity in the $x$-direction, $t$ is the time-dependence variable, $g$ is the gravitational acceleration, $S_0$ $(= tan\,\theta = -\frac{\partial b}{\partial x})$ is the bottom slope source term, $\theta$ is the bottom slope angle, $b$ is the bottom of the non-erodible bed, and $S_f$ is the resistance source term.

### B. Coulomb Resistance

The resistance source term following the Coulomb-type friction law [1, 2, 14] is given as:

$$S_f = cos\,\theta\, tan\,\varphi \quad (3)$$

where $\varphi$ is the internal friction angle of the debris material. Due to the existence of only one internal friction resistance term, Coulomb debris flow may move faster than other types of debris flows, which include more resistance terms, e.g., turbulence, viscosity, and yield stresses, in the resistance source term $S_f$ [2-6].

To ensure a physically realistic debris flow, the right-hand side of (2) must be non-negative [13, 14]. This condition allows the debris flow to propagate from the wet region to the dry region in the initial dam-break problem, thereby triggering the flow condition as:

$$S_0 - S_f \geq 0 \quad \text{or} \quad tan\,\theta - cos\,\theta\, tan\,\varphi \geq 0 \quad (4)$$

This could lead to the application of slope angle $(\theta)$ and internal friction angle $(\varphi)$ as shown in Figure 2.

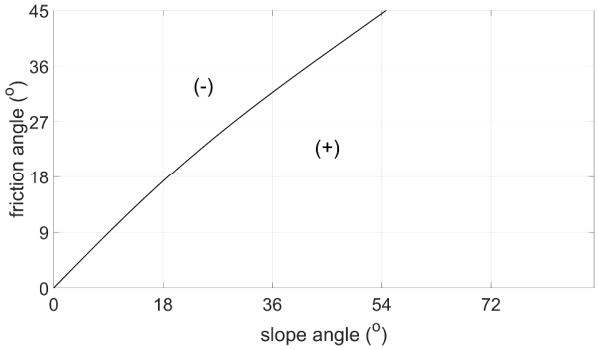


Fig. 2. Application area of slope angle $(\theta)$ and internal friction angle $(\varphi)$ in Coulomb-type friction law for physically realistic debris flow.

The area to the right of the curve, indicated by the symbol (+) to the right of the black solid line in Figure 2, corresponds to physical flow, while the area to the left, indicated by the symbol (-), corresponds to unphysical flow if the Coulomb-type friction law is applied.

### C. Numerical Method

Equations (1) and (2) can be written in conservative form as follows:

$$\frac{\partial U}{\partial t} + \frac{\partial F(U)}{\partial x} = H(U) \quad (5)$$

where:

$$U = \begin{pmatrix} h \\ hu \end{pmatrix}, F(U) = \begin{pmatrix} hu \\ hu^2 + \frac{1}{2} gh^2 \end{pmatrix},$$

$$H(U) = \begin{pmatrix} 0 \\ gh(S_o - S_f) \end{pmatrix} \quad (6)$$

where $U$ is the vector of conserved variables, $U^{\langle 1 \rangle} = h$, and $U^{\langle 2 \rangle} = P = hu$. $F(U)$ and $H(U)$ are the flux and source terms, respectively. Equation (5) is solved using the splitting method for time integration [16]. For spatial integration, the hybrid finite volume-finite difference method is applied [12].

A two-step splitting method is employed to calculate physical variables. The first step is as follows:

$$U_i^{adv} = U_i^n - \frac{\Delta t}{\Delta x}\left[F_{i+1/2} - F_{i-1/2}\right] \quad (7)$$

The physical variable is calculated in the first step as follows:

$$u_i^{adv} = \frac{U_i^{adv}}{h_i^{adv}} \quad (8)$$

The second step is as follows:

$$U_i^{n+1} = U_i^{adv} + \Delta t H(U_i^{adv}) \quad (9)$$

The physical variable is calculated in the second step as follows:

$$u_i^{n+1} = \frac{U_i^{n+1}}{h_i^{adv}} \quad (10)$$

where $h_i^{n+1} = h_i^{adv}$ at the second step because of the non-source term in the continuity equation.

In numerical simulations, the CFL condition is used to ensure stability [12, 14, 19]. In the CFL condition, the Courant number ($0 < CFL < 1$) is chosen to compute the time step $\Delta t$ in the numerical model. The numerical model becomes unstable when the Courant number is large ($CFL > 1$) and stable when the Courant number is small enough ($CFL \approx 0$). However, if the Courant number is too small, it may increase the number of iterations or even cause the model to fail. In this study, the time step is automatically computed after each iteration as follows:

$$\Delta t = CFL \frac{\Delta x}{max(|u|, u_{fn}) + c} \quad (11)$$

where $c$ is the wave celerity and $u_{fn}$ is the friction velocity. Following Coulomb resistance, the friction velocity is calculated as follows:

$$u_{fn} = \sqrt{gh \cos\theta \tan\varphi} \quad (12)$$

### *D. Artificial Bed-Wetting Parameter*

In the first part, the numerical model requires an artificial bed-wetting parameter ($\varepsilon$) in the initial condition, as follows:

$$h = \begin{cases} U^{\langle 1 \rangle} & if\ h > \varepsilon \\ \varepsilon & if\ h \le \varepsilon \end{cases} \quad (13)$$

Then, the particle velocity $u$ is calculated during the step of calculating physical variables as follows:

$$u = \begin{cases} \frac{U^{\langle 2 \rangle}}{h} & if\ h > \varepsilon \\ 0 & if\ h \le \varepsilon \end{cases} \quad (14)$$

Therefore, the particle velocity is always positive in the moving part of the numerical domain and zero in the "quiet" part.

## III. ANALYTICAL SOLUTION FOR COULOMB-TYPE RESISTANCE DEBRIS FLOW

The analytical solution in [13] is used to test the numerical method, as shown in Figure 3.

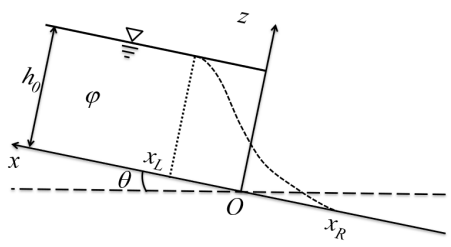


Fig. 3. Schematic of dam-break Coulomb-type debris flow [13].

The debris depth and velocity are calculated as follows:

$$h = \begin{cases} h_0 & if\ x > x_L \\ \frac{\left(\frac{x}{t} + 2c_0 - \frac{1}{2}mt\right)^2}{9g\cos\theta} & if\ x_L \ge x \ge x_R \\ 0 & if\ x \le x_R \end{cases} \quad (15)$$

$$u = \begin{cases} mt & if\ x > x_L \\ \frac{2}{3}\left(\frac{x}{t} - c_0 + mt\right) & if\ x_L \ge x \ge x_R \\ 0 & if\ x < x_R \end{cases} \quad (16)$$

where $x_L = c_0 t + 0.5mt^2$, $x_R = -2c_0 t + 0.5mt^2$, $m$ ($= -g\sin\theta + g\cos\theta\tan\varphi$) is the accelerated source, $c_0$ ($= \sqrt{gh\cos\theta}$) is the sound wave velocity, $\theta$ is the bottom slope angle, and $\varphi$ is the internal friction angle of the material. The analytical solution is used to test the Coulomb-type debris flow numerical model in this study.

## IV. PERFORMANCE OF ARTIFICIAL BED-WETTING PARAMETER

The numerical domain is set to appropriately simulate the dam-break flow based on the analytical solution. The domain in all simulations in this study has a length of 3000 m, with an initial debris depth of $h_0 = 1$ m located on the left side over a half-length segment. No surface friction is considered, as described by the Coulomb-type friction law. In the numerical domain, the left and right boundaries are set with the continuity conditions. The Courant number ($CFL = 0.5$) is taken into account [20] and the computing time is set to 50 s [14]. The grid size of 5 m is chosen to prevent model instabilities and ensure convergence. The artificial bed-wetting parameters are chosen to be equal to or less than 0.1 m until the value that causes the instability of the model due to a large speed of flow.

### *A. Water Dam-Break Test*

The first numerical experiment in this study is the fundamental water dam-break test, conducted on a flatbed ($\theta = 0°$) with water as the material ($\varphi = 0°$) [14, 22-24]. The results of the water dam-break test, including both the analytical solution and numerical simulation, are presented in Table I and Figures 4 and 5.

TABLE I. RESULTS OF WATER DAM-BREAK TEST WITH ARTIFICIAL BED-WETTING PARAMETERS.

| Case | $u_a$ | $\varepsilon$ | $u_f$ | $\frac{\lvert u_f - u_a \rvert}{u_a}$ | RMSE | |
|---|---|---|---|---|---|---|
| | (m/s) | (m) | (m/s) | (%) | for $h$ (m) | for $u$ (m/s) |
| 1 | 6.2641 | $10^{-1}$ | 2.3209 | 63 | 1.2500 | 23.1868 |
| 2 | 6.2641 | $10^{-2}$ | 3.6717 | 41 | 0.2240 | 16.8144 |
| 3 | 6.2641 | $10^{-3}$ | 4.6446 | 26 | 0.0688 | 11.3945 |
| 4 | 6.2641 | $10^{-4}$ | 5.2925 | 16 | 0.0355 | 7.5914 |
| 5 | 6.2641 | $10^{-5}$ | 5.6436 | 10 | 0.0308 | 5.3974 |

In Table I, $u_a$ denotes the front velocity (the maximum velocity of the analytical solution), and $\varepsilon$ is the artificial bed-wetting parameter. Additionally, $u_f$ denotes the front velocity (or maximum speed) obtained from the numerical simulation, and RMSE refers to the Root Mean Square Error. RMSE is calculated to quantify the cumulative error of both debris depth

and debris velocity between the numerical results and the analytical solution [19]. Figures 4 and 5 illustrate the performance of artificial bed-wetting parameters based on the flow characteristics from Table I.

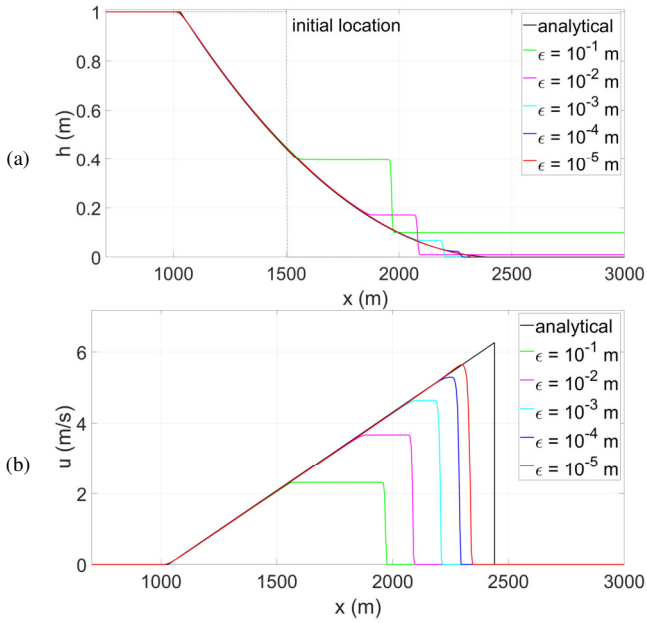


Fig. 4. Performance of artificial bed-wetting parameters in water dam-break test: (a) water depth, (b) water velocity. (The black line represents the analytical solution; the green line corresponds to the case of $\varepsilon = 10^{-1}$ m, the magenta line corresponds to the case of $\varepsilon = 10^{-2}$ m, the cyan line corresponds to the case of $\varepsilon = 10^{-3}$ m, the blue line corresponds to the case of $\varepsilon = 10^{-4}$ m, the red line corresponds to the case of $\varepsilon = 10^{-5}$ m).

Figure 4 shows the water depth (a) and water velocity (b) from both analytical solution and numerical results with various artificial bed-wetting parameters across the domain. In general, the inclusion of artificial bed-wetting parameters at the downstream side of the dam in the numerical domain causes the shock wave phenomenon, affecting the front surface and front velocity, as depicted in Figure 4 (a) and (b), respectively. The value of the artificial bed-wetting parameters influences the front surface size, with larger values ($\varepsilon = 10^{-1}$ m) resulting in a larger front surface, and smaller values ($\varepsilon = 10^{-5}$ m) resulting in a smaller front surface. In the analytical solution, the downstream region has no depth, and the results are smooth and consistent with the physical phenomenon. These findings indicate that the best results are obtained with $\varepsilon = 10^{-5}$ m. However, using smaller values of $\varepsilon$ can lead to instabilities in the numerical model.

Figure 5 shows the performance of the artificial bed-wetting parameter in relation to the front velocity and RMSE of $h$ and $u$. Similar to the results in [16], the relationship between the artificial bed-wetting parameter and front velocity is shown in Figure 5(a). As $\varepsilon$ decreases, the front velocity increases. The best value of $\varepsilon = 10^{-5}$ m results in a front velocity $u_f = 5.6436$ m/s with a 10% difference from the analytical value $u_a = 6.2641$ m/s. Figure 5(b) shows the errors in water depth and velocity profile between numerical results and the analytical solution for different relative artificial bed-wetting parameters. As the relative artificial bed-wetting parameter decreases, the RMSE values for both $h$ and $u$ decrease. Additionally, the RMSE values for $u$ are much larger than those for $h$, ranging from about 20 to 200 times larger.

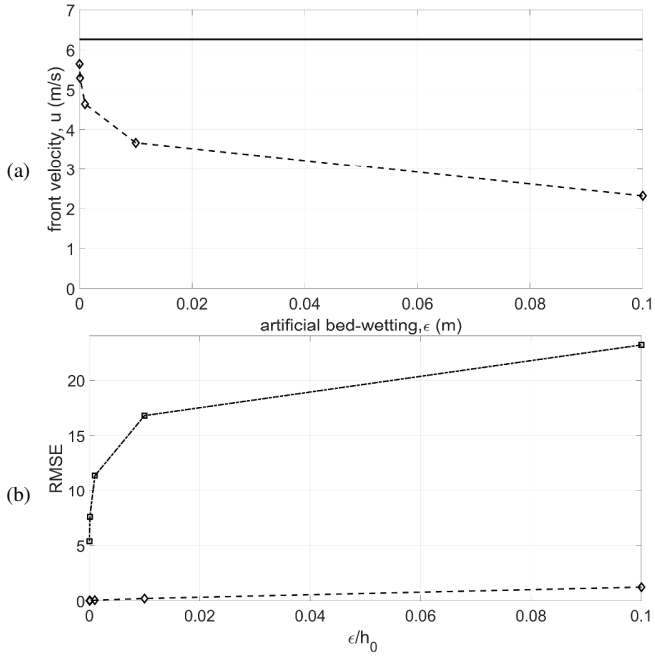


Fig. 5. Performance of artificial bed-wetting parameter in terms of front velocity and RMSE for $h$ and $u$ in water dam-break test: (a) Performance of artificial bed-wetting parameter to water-front velocity (dashed line: numerical results, solid line: analytical solution), (b) Performance of relative artificial bed-wetting parameter to RMSE (dashed line: RMSE value of $h$, dashed-dot line: RMSE value of $u$).

### *B. Performance of Artificial Bed-Wetting Parameters with Slopes*

To ensure that the physical behavior is consistent with Coulomb friction, the slope angle of the domain must exceed the internal friction angle of the material, as described in [13] and illustrated in Figure 2. In this subsection, artificial bed-wetting parameters are analyzed for slopes with angles of 2.5° and 5°, while assuming an internal friction angle of $\varphi = 0°$ (water material). Figure 6 and Table II present the results for the 2.5° slope under varying artificial bed-wetting conditions. Similarly, Table III and Figure 7 detail the results for the 5° slope.

In Table II, the front velocity values of the numerical model for the slope case of $\varepsilon = 2.5°$ closely match those of the analytical solution, resulting in differences ($\frac{|u_f - u_a|}{u_a}(\%)$) that are approximately half of those observed on a flatbed. However, the RMSE values for $u$ in this case are larger, which can be attributed to differences in the shapes of the velocity profiles. Figure 6 illustrates the performance of artificial bed-wetting parameters for a slope angle of $\varepsilon = 2.5°$, focusing on water depth and velocity. The larger shock wave fronts induced by the slope angle ($\theta = 2.5°$) lead to instabilities in the water

depth, as shown in Figure 6(a). In this case, the effect of the source term, the right-hand side of (2) at the second step, generates a potential velocity component upstream of the dam, near the shock front, with values slightly lower than the front velocity [Figure 6(b)]. Additionally, due to the same source term effect, tail velocity values are observed on the right side of the shock front, corresponding to the artificial bed-wetting parameter $h = \varepsilon$ (m).

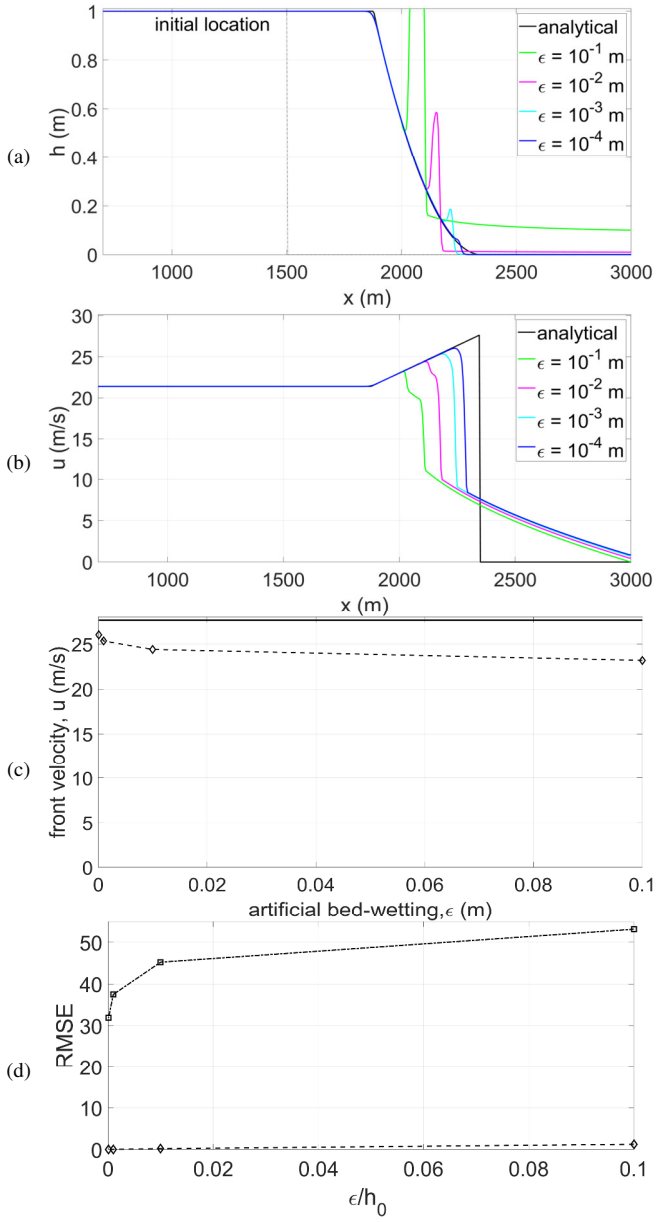


Fig. 6. Performance of artificial bed-wetting parameter in case of slope angle $\theta = 2.5°$ on water dam-break test: (a) debris depth, (b) debris velocity, (c) Performance of artificial bed-wetting parameter to water-front velocity (dashed line: numerical results, solid line: analytical solution), (d) Performance of relative artificial bed-wetting parameter to RMSE (dashed line: RMSE value of $h$, dashed-dot line: RMSE value of $u$).

TABLE II. RESULTS OF WATER DAM-BREAK TEST OF SLOPE $\theta = 2.5°$ WITH ARTIFICIAL BED-WETTING PARAMETER

| Case | $u_a$ | $\varepsilon$ | $u_f$ | $\frac{\lvert u_f - u_a \rvert}{u_a}$ | RMSE | |
|---|---|---|---|---|---|---|
| | (m/s) | (m) | (m/s) | (%) | for $h$ (m) | for $u$ (m/s) |
| 1 | 27.6559 | $10^{-1}$ | 23.1882 | 16 | 1.2816 | 53.1390 |
| 2 | 27.6559 | $10^{-2}$ | 24.4006 | 12 | 0.2311 | 45.2391 |
| 3 | 27.6559 | $10^{-3}$ | 25.3372 | 8 | 0.0585 | 37.5078 |
| 4 | 27.6559 | $10^{-4}$ | 26.0245 | 6 | 0.0229 | 31.9349 |

Figure 6(c) shows larger values of front velocity compared to the flatbed with the same artificial bed-wetting values. However, these values seem closer to the analytical front velocity with a maximum difference of 16% compared to 63% of the flatbed. This is also more remarkable for the difference of RMSE values of $u$ and $h$ with a maximum of 1400 times in Figure 6(d).

Figure 6(c) shows that the front velocity values for the slope case are larger compared to the flatbed when using the same artificial bed-wetting values. However, these values are closer to the analytical front velocity, with a maximum difference of 16%, compared to 63% for the flatbed. When comparing the RMSE values of $u$ and $h$, as shown in Figure 6(d), the maximum observed difference is as high as 1400 times.

These observations become even more pronounced when the slope angle $\theta$ increases to 5°, compared to the results of the slope angle of 0° in Table I and the slope angle of 2.5° in Table II, as shown in Table III and Figure 7.

TABLE III. RESULTS OF WATER DAM-BREAK TEST OF $\theta$ = 5° WITH ARTIFICIAL BED-WETTING PARAMETER

| Case | $u_a$ | $\varepsilon$ | $u_f$ | $\frac{\lvert u_f - u_a \rvert}{u_a}$ | RMSE | |
|---|---|---|---|---|---|---|
| | (m/s) | (m) | (m/s) | (%) | for $h$ (m) | for $u$ (m/s) |
| 1 | 49.0013 | $10^{-1}$ | 43.5242 | 11 | 1.5554 | 99.3538 |
| 2 | 49.0013 | $10^{-2}$ | 45.2122 | 8 | 0.3830 | 74.3311 |
| 3 | 49.0013 | $10^{-3}$ | 46.3415 | 5 | 0.1022 | 52.3121 |
| 4 | 49.0013 | $10^{-4}$ | 47.1658 | 4 | 0.0523 | 37.2969 |

In Table III, the front velocity values show a slight difference from the analytical solution, ranging from 4% to 11%. Additionally, the RMSE values of $u$ and $h$ exhibit significant differences, attributed to the increasing influence of the source term.

The instability of the shock front is shown in Figure 7(a), while Figure 7(b) highlights the increase in both potential and tail velocities. In Figure 7(c), the front velocity values align more closely with the analytical solution, reaching a maximum value of 47.1658 m/s. With the absence of internal friction resistance in the source term ($\varphi = 0°$), this presents the maximum debris velocity observed in this study. Additionally, Figure 7(d) demonstrates significant differences between the RMSE values of $u$ and $h$.

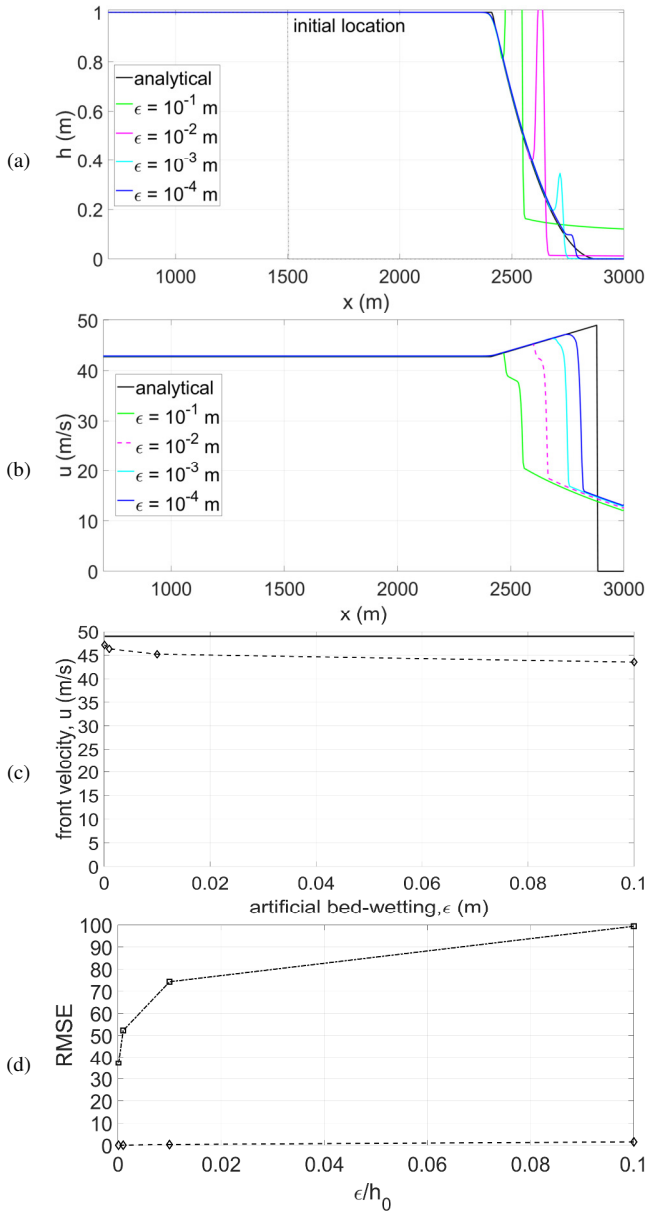


Fig. 7. Performance of artificial bed-wetting parameters in case of slope angle $\theta$ = 5° in water dam-break test: (a) debris depth, (b) debris velocity, (c) Performance of artificial bed-wetting parameter to water-front velocity (dashed line: numerical results, solid line: analytical solution), (d) Performance of relative artificial bed-wetting parameter to RMSE (dashed line: RMSE value of $h$, dashed-dot line: RMSE value of $u$).

By analyzing the performance of artificial bed-wetting parameters for slope angles $\theta$ = 0°, 2.5°, and 5°, Figure 8 illustrates the relationship between slope angle and front velocity under varying artificial bed-wetting conditions. This figure shows that the front velocities generally increase with higher slope angles, regardless of the value of $\varepsilon$. Additionally, as $\varepsilon$ decreases, the front velocities increase and become closer to the analytical solutions. For each value of $\varepsilon$, a linear regression is established, with the resulting lines running parallel to the analytical solution line. These linear regression equations are presented in Table IV.

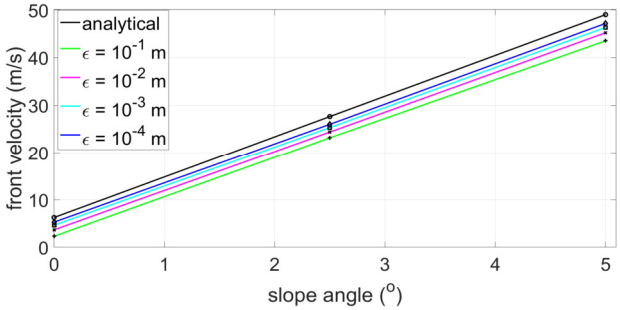


Fig. 8. Performance of artificial bed-wetting parameter in the relationship between slope and front velocity in case of internal friction angle $\varphi$ = 0°.

TABLE IV. LINEAR REGRESSION EQUATIONS FOR THE RELATIONSHIP BETWEEN SLOPE AND FRONT VELOCITY WITH THE PERFORMANCE OF ARTIFICIAL BED-WETTING PARAMETER

| Case | $\varepsilon_h$ (m) | a | b | $R^2$ | Linear equation (m/s) |
|---|---|---|---|---|---|
| 1 | $10^{-1}$ | 8.241 | 2.410 | 0.999 | $u_f = 8.241\theta' + 2.410$ |
| 2 | $10^{-2}$ | 8.308 | 3.658 | 1 | $u_f = 8.308\theta' + 3.658$ |
| 3 | $10^{-3}$ | 8.339 | 4.593 | 1 | $u_f = 8.339\theta' + 4.593$ |
| 4 | $10^{-4}$ | 8.375 | 5.224 | 1 | $u_f = 8.375\theta' + 5.224$ |
| 5 | Analytical | 8.547 | 6.272 | 1 | $u_f = 8.547\theta' + 6.272$ |

## C. *Performance of Artificial Bed-Wetting Parameters with Frictions*

To ensure the physical flow in the Coulomb-type numerical model, the slope angle of $\theta$ =5° is kept constant, with internal friction angles of $\varphi$ = 2° and 4°. Table V - Figure 9, and Table VI - Figure 10, present the results of the debris dam-break test for $\varphi$ = 2° and 4°, respectively. As mentioned earlier, with the existence of the resistance source term ($-tan\,\varphi\,cos\,\theta$), the values of the front velocity decrease as the internal friction angle increases from 2° to 4°, compared to the case with an internal friction angle of 0°.

TABLE V. RESULTS OF DEBRIS DAM-BREAK TEST OF $\varphi$ = 2° WITH ARTIFICIAL BED-WETTING PARAMETER

| Case | $u_a$ | $\varepsilon$ | $u_f$ | $\frac{\lvert u_f - u_a \rvert}{u_a}$ | RMSE | |
|---|---|---|---|---|---|---|
| | (m/s) | (m) | (m/s) | (%) | for $h$ (m) | for $u$ (m/s) |
| 1 | 31.9377 | $10^{-1}$ | 27.4242 | 14 | 1.3343 | 68.1716 |
| 2 | 31.9377 | $10^{-2}$ | 28.7126 | 10 | 0.2733 | 57.5336 |
| 3 | 31.9377 | $10^{-3}$ | 29.6356 | 7 | 0.0753 | 47.0150 |
| 4 | 31.9377 | $10^{-4}$ | 30.3730 | 5 | 0.0434 | 39.8456 |

There are still shock fronts occurring in debris depth at Figure 9(a), which cause the RMSE value of $h$ to reach a maximum value of 1.3343 m in Table V. The differences in front velocities from the analytical solution are relatively small (with a maximum value of 14%), while the differences in the velocity profile are relatively large (with a maximum value of 68.1716), as shown in Figure 9(b, c, d).

Compared to the case of $\varphi$ =2°, most values in the case of $\varphi$ = 4° are increased, except for the differences between front velocity and analytical solution, as shown in Table VI and Figure 10.

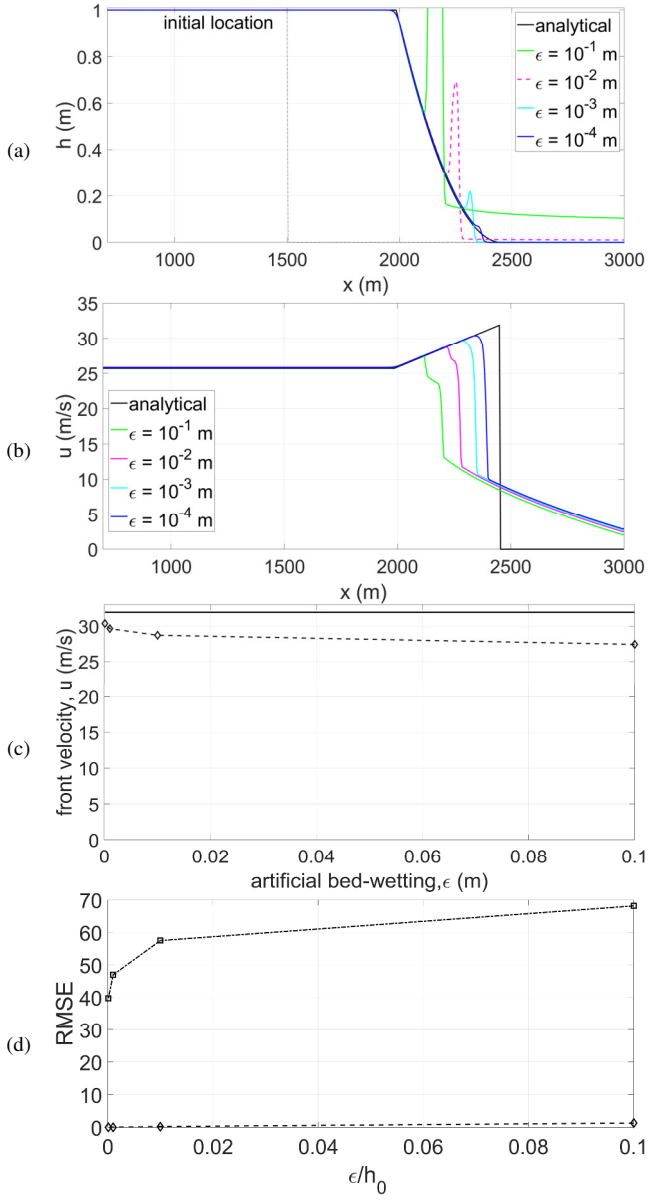


Fig. 9. Performance of artificial bed-wetting parameters in case of friction angle $\varphi$ = 2° in water dam-break test: (a) debris depth, (b) debris velocity, (c) Performance of artificial bed-wetting parameter to water-front velocity (dashed line: numerical results, solid line: analytical solution), (d) Performance of relative artificial bed-wetting parameter to RMSE (dashed line: RMSE value of $h$, dashed-dot line: RMSE value of $u$).

TABLE VI. RESULTS OF DEBRIS DAM-BREAK TEST OF $\varphi$ = 4° WITH ARTIFICIAL BED-WETTING PARAMETERS

| Case | $u_a$ | $\varepsilon$ | $u_f$ | $\frac{\lvert u_f - u_a \rvert}{u_a}$ | RMSE | |
|---|---|---|---|---|---|---|
| | (m/s) | (m) | (m/s) | (%) | for $h$ (m) | for $u$ (m/s) |
| 1 | 14.833 | $10^{-1}$ | 10.9212 | 26 | 1.2658 | 21.8885 |
| 2 | 14.833 | $10^{-2}$ | 12.1023 | 18 | 0.1977 | 18.3402 |
| 3 | 14.833 | $10^{-3}$ | 13.0163 | 12 | 0.0698 | 15.2487 |
| 4 | 14.833 | $10^{-4}$ | 13.6439 | 8 | 0.0518 | 12.9529 |
| 5 | 14.833 | $10^{-5}$ | 13.8565 | 7 | 0.0433 | 11.2049 |

Due to friction, the front velocity and RMSE values decrease, but the differences between numerical and analytical front velocity increase, with a maximum value of 26%. As a result, the shock fronts become stable in the debris depth [Figure 10(a)], and the potential as well as tail velocities do not show an advantage [Figure 10(b)].

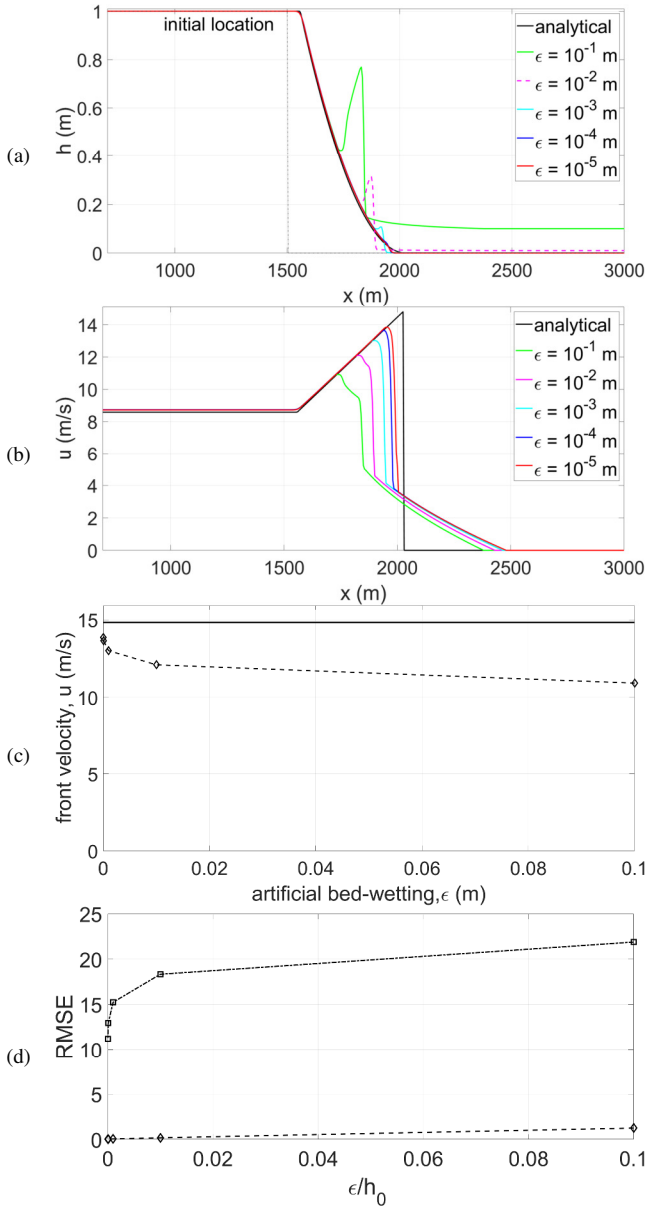


Fig. 10. Performance of artificial bed-wetting parameters in case of friction angle $\varphi$ = 4° on debris dam-break test of $\theta$ = 5°: (a) debris depth, (b) debris velocity, (c) Performance of artificial bed-wetting parameter to water-front velocity (dashed line: numerical results, solid line: analytical solution), (d) Performance of relative artificial bed-wetting parameter to RMSE (dashed line: RMSE value of $h$, dashed-dot line: RMSE value of $u$).

Figure 10(c) shows large differences between front velocities and the analytical solution, while Figure 10(d) shows small differences between the RMSE of $u$ and $h$.

Figure 11 shows the performance of friction on the values of front velocities with different artificial bed-wetting parameters. For each case of $\varepsilon$, the front velocity values decrease as the internal friction angle increases. This behavior has physical significance due to the resistance effect in flow.

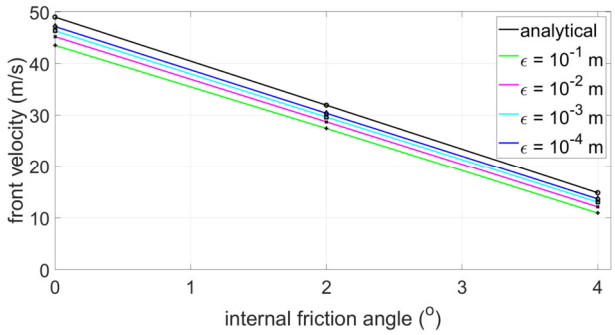


Fig. 11. Performance of artificial bed-wetting parameters in the relationship between friction and front velocity in case of slope angle $\theta$=5°.

Similarly, the relationship between internal friction angles and front velocities is linear, and it can be expressed by the linear equations shown in Table VII.

TABLE VII. LINEAR REGRESSION EQUATIONS FOR THE RELATIONSHIP BETWEEN FRICTION AND FRONT VELOCITY WITH THE PERFORMANCE OF ARTIFICIAL BED-WETTING PARAMETERS

| Case | $\varepsilon_h$ (m) | a | b | $R^2$ | Linear equation (m/s) |
|---|---|---|---|---|---|
| 1 | $10^{-1}$ | -8.151 | 43.591 | 0.999 | $u_f$ = -8.151$\varphi^o$ +43.591 |
| 2 | $10^{-2}$ | -8.278 | 45.231 | 1 | $u_f$ = -8.278$\varphi^o$ +45.231 |
| 3 | $10^{-3}$ | -8.331 | 46.327 | 1 | $u_f$ = -8.331$\varphi^o$ +46.327 |
| 4 | $10^{-4}$ | -8.381 | 47.155 | 1 | $u_f$ = -8.381$\varphi^o$ +47.155 |
| 5 | Analytical | -8.542 | 49.008 | 1 | $u_f$ = -8.542$\varphi^o$ +49.008 |

### *D. Discussion*

Overall, the best value for the artificial bed-wetting parameter in this study is $10^{-4}$ m, except for the value of $10^{-5}$ m in cases of the minimum and maximum value of ($\theta$, $\varphi$). These special cases are more stable than the others due to the balance between the positive slope term and the negative friction term in the source term, leading to slower movement of the debris near the initial dam [14]. These artificial bed-wetting parameters also result in small differences in front velocities between numerical and analytical solutions, which are less than or equal to 10 %, as shown in Tables I, II, III, V, and VI. If smaller values of these artificial bed-wetting parameters are used, the front velocities may increase sharply, causing very small time steps, which in turn may lead to numerical instabilities after a few iterations. In other debris models, smaller values of the artificial bed-wetting parameter are considered due to the application of the implicit method in calculating turbulent resistance.

The difference in front velocity between the numerical and analytical solution decreases as the slope angle $\theta$ increases and the internal friction angle $\varphi$ decreases, regardless of the values of the artificial bed-wetting parameters, as shown in Tables II, III, IV, and V. This is due to the dominance of the slope source term compared to the friction source term on the right-hand side of (2), which affects the updating of only the particle velocity variable in (9) and (10). However, this observation is obtained only for the font velocity or maximum speed. For the velocity profile, it can be quantified using the RMSE of $u$.

Despite the smallest difference in front velocity, at 4 %, for the water case with $\varepsilon = 10^{-4}$ m and a slope of $\theta$ = 5°, the RMSE of $u$ is significantly large in this case, with a value of 37.2969 m. This large RMSE arises from the accumulation of particle velocity in the differing front shapes, which results from the existence of debris depth in the source term, as mentioned earlier. In real application, the choice between focusing on the front velocity value or the particle velocity profile depends on the specific research purpose.

## V. CONCLUSIONS

This study investigated the performance of artificial bed-wetting parameters with physical variables on various slopes and frictions in a Coulomb-type 1D debris flow model. The governing equations of the 1D debris flow model, using debris depth and velocity as physical variables, were presented. The bottom slope and Coulomb resistance, incorporating only the internal friction term, were used as the source terms in this debris model. The slope angle and the internal friction angle ranges were defined to ensure the physical direction of debris flow. In the numerical solution, the artificial bed-wetting parameter is required to ensure numerical stability in the debris model when computing physical variables. The results for debris depth and front velocity were demonstrated through five dam-break debris tests with different values of the artificial bed-wetting parameter. These results were analyzed based on the performance of the artificial bed-wetting parameters with respect to slopes and frictions. For the case with the highest slope angle and the lowest internal friction angle, the front velocities of the numerical model and analytical solution are the closest. Consequently, an inverse relationship was established between slope angles and front velocities, while a reverse relationship was observed between internal friction angles and front velocities. These findings are physically reasonable in general and can be used to predict debris flow properties in field applications. Future work will consider other resistance relationships in the source term of the numerical debris model to more broadly model real landslide phenomena.

## ACKNOWLEDGMENT

This research was funded by Vietnam Maritime University.

## REFERENCES

[1] S. B. Savage and K. Hutter, "The motion of a finite mass of granular material down a rough incline," *Journal of Fluid Mechanics*, vol. 199, pp. 177–215, Feb. 1989, https://doi.org/10.1017/S0022112089000340.

[2] D. Naef, D. Rickenmann, P. Rutschmann, and B. W. McArdell, "Comparison of flow resistance relations for debris flows using a one-dimensional finite element simulation model," *Natural Hazards and Earth System Sciences*, vol. 6, no. 1, pp. 155–165, Feb. 2006, https://doi.org/10.5194/nhess-6-155-2006.

[3] V. Medina, M. Hürlimann, and A. Bateman, "Application of FLATModel, a 2D finite volume code, to debris flows in the northeastern part of the Iberian Peninsula," *Landslides*, vol. 5, no. 1, pp. 127–142, Feb. 2008, https://doi.org/10.1007/s10346-007-0102-3.

[4] H. X. Chen and L. M. Zhang, "EDDA 1.0: integrated simulation of debris flow erosion, deposition and property changes," *Geoscientific Model Development*, vol. 8, no. 3, pp. 829–844, Mar. 2015, https://doi.org/10.5194/gmd-8-829-2015.

[5] C. Ouyang, S. He, and C. Tang, "Numerical analysis of dynamics of debris flow over erodible beds in Wenchuan earthquake-induced area," *Engineering Geology*, vol. 194, pp. 62–72, Aug. 2015, https://doi.org/10.1016/j.enggeo.2014.07.012.

[6] P. Shen, L. Zhang, H. Chen, and R. Fan, "EDDA 2.0: integrated simulation of debris flow initiation and dynamics considering two initiation mechanisms," *Geoscientific Model Development*, vol. 11, no. 7, pp. 2841–2856, Jul. 2018, https://doi.org/10.5194/gmd-11-2841-2018.

[7] S. Jeong, Y. Kim, J. K. Lee, and J. Kim, "The 27 July 2011 debris flows at Umyeonsan, Seoul, Korea," *Landslides*, vol. 12, no. 4, pp. 799–813, Aug. 2015, https://doi.org/10.1007/s10346-015-0595-0.

[8] R. M. Iverson, M. Logan, R. G. LaHusen, and M. Berti, "The perfect debris flow? Aggregated results from 28 large-scale experiments," *Journal of Geophysical Research: Earth Surface*, vol. 115, Sep. 2010, Art. no. 2009JF001514, https://doi.org/10.1029/2009JF001514.

[9] R. M. Iverson, M. E. Reid, M. Logan, R. G. LaHusen, J. W. Godt, and J. P. Griswold, "Positive feedback and momentum growth during debris-flow entrainment of wet bed sediment," *Nature Geoscience*, vol. 4, no. 2, pp. 116–121, Feb. 2011, https://doi.org/10.1038/ngeo1040.

[10] R. P. Denlinger and R. M. Iverson, "Flow of variably fluidized granular masses across three-dimensional terrain: 2. Numerical predictions and experimental tests," *Journal of Geophysical Research: Solid Earth*, vol. 106, no. B1, pp. 553–566, Jan. 2001, https://doi.org/10.1029/2000JB900330.

[11] S. McDougall and O. Hungr, "Dynamic modelling of entrainment in rapid landslides," *Canadian Geotechnical Journal*, vol. 42, no. 5, pp. 1437–1448, Oct. 2005, https://doi.org/10.1139/t05-064.

[12] V. K. Pham, C. Lee, and V. N. Vu, "Numerical Simulation of Subaerial and Submarine Landslides Using the Finite Volume Method in the Shallow Water Equations with (*b*, *s*) Coordinate," *Journal of Korean Society of Coastal and Ocean Engineers*, vol. 31, no. 4, pp. 229–239, Aug. 2019, https://doi.org/10.9765/KSCOE.2019.31.4.229.

[13] A. Mangeney, P. Heinrich, and R. Roche, "Analytical Solution for Testing Debris Avalanche Numerical Models," *Pure and Applied Geophysics*, vol. 157, no. 6–8, pp. 1081–1096, Aug. 2000, https://doi.org/10.1007/s000240050018.

[14] J. Paik, "A high resolution finite volume model for 1D debris flow," *Journal of Hydro-environment Research*, vol. 9, no. 1, pp. 145–155, Mar. 2015, https://doi.org/10.1016/j.jher.2014.03.001.

[15] M. Peruzzetto *et al.*, "Simplified simulation of rock avalanches and subsequent debris flows with a single thin-layer model: Application to the Prêcheur river (Martinique, Lesser Antilles)," *Engineering Geology*, vol. 296, Jan. 2022, Art. no. 106457, https://doi.org/10.1016/j.enggeo.2021.106457.

[16] E. F. Toro and E. Toro, *Shock-Capturing Methods for Free-Surface Shallow Flows*, 1st ed. Chichester: Wiley, 2001.

[17] Q. Liang and A. G. L. Borthwick, "Adaptive quadtree simulation of shallow flows with wet–dry fronts over complex topography," *Computers & Fluids*, vol. 38, no. 2, pp. 221–234, Feb. 2009, https://doi.org/10.1016/j.compfluid.2008.02.008.

[18] C. Xia, Z. Cao, G. Pender, and A. Borthwick, "Numerical algorithms for solving shallow water hydro-sediment-morphodynamic equations," *Engineering Computations*, vol. 34, no. 8, pp. 2836–2861, Nov. 2017, https://doi.org/10.1108/EC-01-2016-0026.

[19] X. Xia and Q. Liang, "A new efficient implicit scheme for discretising the stiff friction terms in the shallow water equations," *Advances in Water Resources*, vol. 117, pp. 87–97, Jul. 2018, https://doi.org/10.1016/j.advwatres.2018.05.004.

[20] J. Hou *et al.*, "An implicit friction source term treatment for overland flow simulation using shallow water flow model," *Journal of Hydrology*, vol. 564, pp. 357–366, Sep. 2018, https://doi.org/10.1016/j.jhydrol.2018.07.027.

[21] L. Lu, Y. Chen, M. Li, H. Zhang, and Z. Liu, "Robust well-balanced method with flow resistance terms for accurate wetting and drying modeling in shallow water simulations," *Advances in Water Resources*, vol. 191, Sep. 2024, Art. no. 104760, https://doi.org/10.1016/j.advwatres.2024.104760.

[22] C. Ancey, R. M. Iverson, M. Rentschler, and R. P. Denlinger, "An exact solution for ideal dam-break floods on steep slopes," *Water Resources Research*, vol. 44, no. 1, Jan. 2008, Art. no. 2007WR006353, https://doi.org/10.1029/2007WR006353.

[23] F. Bai, Z. Yang, and W. Zhou, "Study of total variation diminishing (TVD) slope limiters in dam-break flow simulation," *Water Science and Engineering*, vol. 11, no. 1, pp. 68–74, Jan. 2018, https://doi.org/10.1016/j.wse.2017.09.004.

[24] A. Benabid, M. Badis, F. Ali, M. Tarek, and M. Saadi, "Numerical Simulation of Gradually Varying Permanent Flows in a Prismatic Open Channel for Four Geometric Shapes," *Engineering, Technology & Applied Science Research*, vol. 14, no. 4, pp. 15274–15282, Aug. 2024, https://doi.org/10.48084/etasr.7715.